Optimizing Single-Walled-Carbon-Nanotube-Based Saturable Absorbers for Ultrafast Lasers

*Stefania Ferrari, Marcella Bini, Doretta Capsoni, Pietro Galinetto, Marco Simone Grandi, Uwe Griebner, Günter Steinmeyer, Antoniangelo Agnesi, Federico Pirzio, Elena Ugolotti, Giancarlo Reali, and Vincenzo Massarotti**

The application of single-walled carbon nanotubes (SWCNTs) as saturable absorbers (SA) in a Nd:glass femtosecond laser is verified as a promising alternative to traditional semiconductor saturable-absorber mirrors (SESAMs). The shortest laser pulses achieved with a SWCNT-SA fabricated by the slow-evaporation method are reported herein. Nearly Fourier-limited 288 fs pulses are obtained with negative-dispersion soliton mode-locking. The importance of the properties of the starting material, such as the degree of purity and the chirality, and the successive slow-evaporation deposition method is proven by using a multitechnique approach based on X-ray diffractometry, scanning electron microscopy, and μ-Raman spectroscopy. The high degree of nanotube alignment on the glass substrate and also the slight metallic character due to electron transfer between the glass matrix and the nanotubes themselves are identified as the main features responsible for the good laser response.

1. Introduction

In the ultrafast photonics field, there has been growing interest observed in recent years in the development of new devices capable of a high yield, with low-cost manufacture, but delivering a high performance and with unique functionality. Femtosecond technology based on mode-locked solid-state or fiber laser sources is of great importance in academic, biomedical, and industrial applications. At present, semiconductor saturable-absorber mirrors (SESAMs) are largely employed in mode-locked solid-state lasers operating over a broad spectral range.[1] However, SESAMs present numerous drawbacks, such as a spectrally narrowband non-linearity and, more importantly, their fabrication requires a very sophisticated and expensive manufacturing process. For these reasons, research is now devoted to the development of new saturable absorbers based on materials with pronounced optical non-linearity, a high optical damage threshold, a broad operating range, and simple production processes. Recent progress in nanotechnology has made it possible to overcome many of the problems of traditional SESAMs and offers new materials that can be used in solid-state lasers. Ideal candidates for such applications are graphene and carbon nanotubes,[2–4] although their commercial applications are currently restricted to mode-locking fiber lasers that are sufficiently tolerant towards non-saturable losses.[5] In particular, single-walled carbon nanotubes (SWCNTs) exhibit strong optical absorption in a broad spectral range from the UV to the near-IR depending on their mean diameter; they have unique third non-linear optical properties, are chemically stable and mechanically robust, and they possess a very high optical-damage threshold. Only very small quantities of SWCNTs are necessary to assemble photonic devices and thus low production costs can be easily achieved. All of these interesting characteristics make SWCNTs promising for their application in solid-state lasers. The performance of SWCNT saturable absorbers (SWCNT-SAs) is strongly influenced by the curling of the nanotubes, which easily form bundles that can produce significant scattering losses, inhibiting mode-locking.[3] Therefore, close attention has to be paid during the preparation steps (dispersion, film deposition, etc.) of SWCNT-SAs.

The aim of this work is the development of a saturable absorber based on a film of SWCNTs deposited on a quartz substrate by the slow-evaporation method.[6] With respect to spin-coating a glass substrate with SWCNTs dispersed in a polymeric solution, evaporation looks promising since it does not make use of the polymer; therefore, the SA obtained in

Dr. S. Ferrari, Dr. M. Bini, Dr. D. Capsoni, Prof. V. Massarotti
Department of Chemistry
University of Pavia
Via Taramelli 16, 27100 Pavia
E-mail: vincenzo.massarotti@unipv.it
Dr. P. Galinetto, Dr. M. S. Grandi
Department of Physics
University of Pavia
Via Bassi, 27100 Pavia
Dr. U. Griebner, Dr. G. Steinmeyer
Max-Born-Institute for Nonlinear Optics and Ultrafast Spectroscopy
2A-Max-Borrn Str., 12489 Berlin, Germany
Prof. A. Agnesi, Dr. F. Pirzio, E. Ugolotti, Prof. G. Reali
Department of Electronics
University of Pavia
Via Ferrata 1, 27100 Pavia

DOI: 10.1002/adfm.201200157

this way can be applied to high-power lasers as well.[7] Our attention has been focused on the physico-chemical characterization of the carbon nanotubes before and after the purification process, in order to demonstrate the crucial role of the preparation method on their successive application. Different characterization techniques have been employed: scanning electron microscopy (SEM) with energy-dispersion spectroscopy (EDS), X-ray powder diffraction (XRPD) and μ-Raman spectroscopy. In particular, Raman spectroscopy is a useful tool for the investigation of the properties of carbon nanotubes and features both as powder and deposited film as saturable absorbers. In the early 90s, Nd:glass was the first diode-pumped solid-state laser reported generating femtosecond pulses, using SESAM passive mode-locking.[8] It is still attractive because of its simplicity and reliable mode-locking operation at low pump power levels. New, effective design solutions have been recently reported, employing efficient single-mode pumped resonators.[9] Therefore, for all these reasons, our SWCNT-SA has been tested using a Nd:glass femtosecond laser to verify the mode-locking performance of the nanotube film.

2. Results and Discussion

Different techniques were used at first to verify the degree of purity of the commercial nanotubes, considering that traces of impurities can affect the subsequent application in lasers. In **Figure 1**a, a SEM image is shown relative to a commercial sample. A big aggregate of carbonaceous material is well evident and the typical morphology of nanotubes does not appear, even on dramatically increasing the magnification. This image also shows the presence of several bright, octahedral crystallites, whose magnification is shown in Figure 1c. EDS analysis performed on these bright crystallites allowed us to identify the elemental composition of these impurities, which are made up of molybdenum (Figure 1b). A more general survey of the sample also revealed the presence of cobalt and traces of other elements. The same impurities were also revealed by XRPD; the patterns of the commercial and purified samples are reported in **Figure 2**. The diffractogram of the pristine sample (trace a) shows many reflections due to impurity phases, such as metallic cobalt and molybdenum, cobalt halides, and also some phases that are difficult to determine, together with the (002)

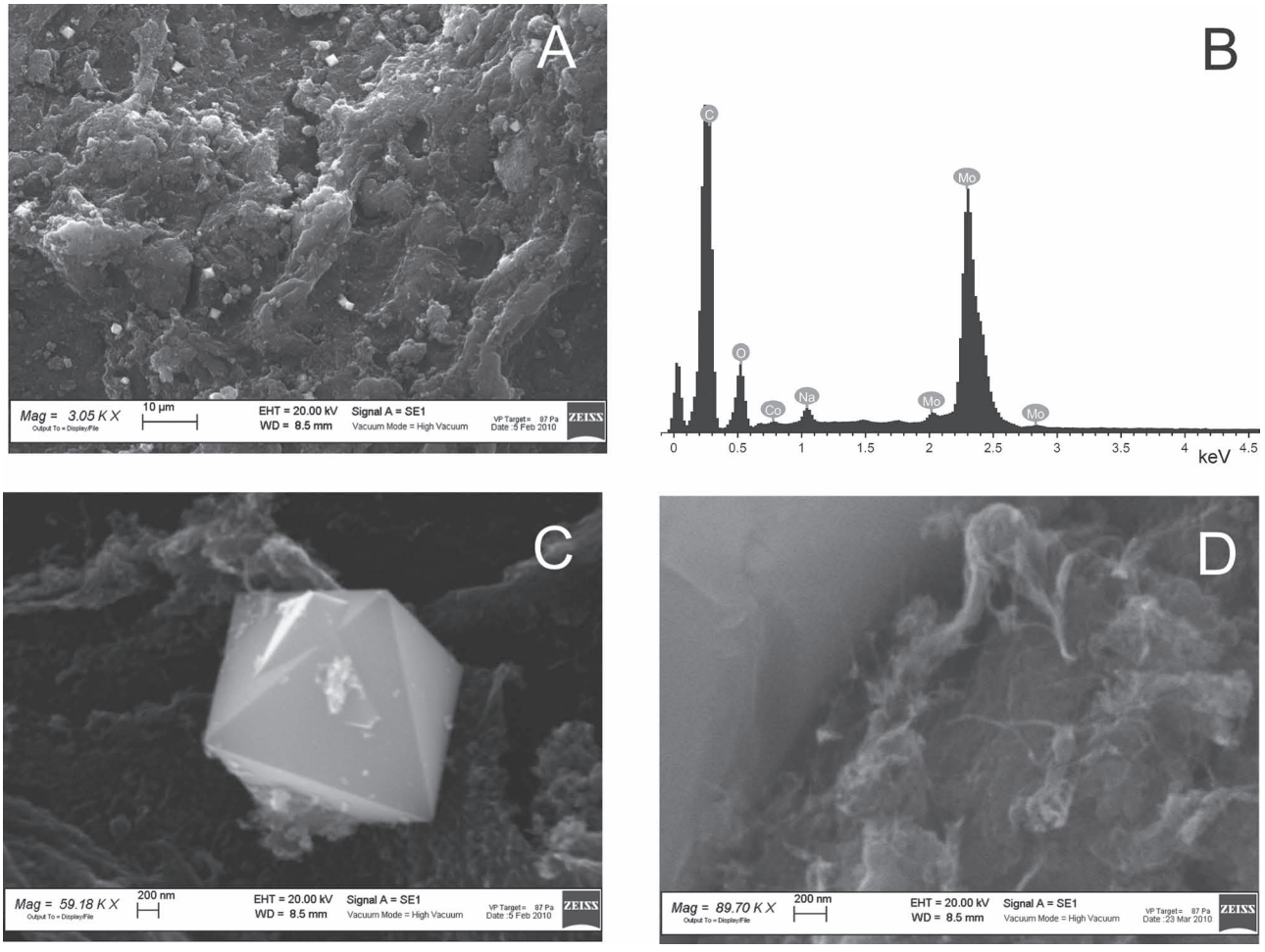

Figure 1. a) SEM image of a commercial SWCNT sample. b) Relative EDS analysis of the commercial SWCNT sample. c) Magnified SEM image of the bright particles present in (a). d) SEM image of the purified nanotubes.

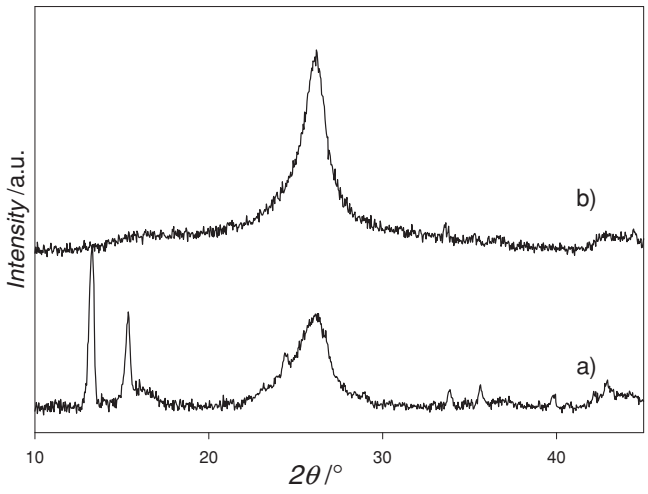

Figure 2. XRPD patterns of the a) commercial and b) purified carbon-nanotube samples.

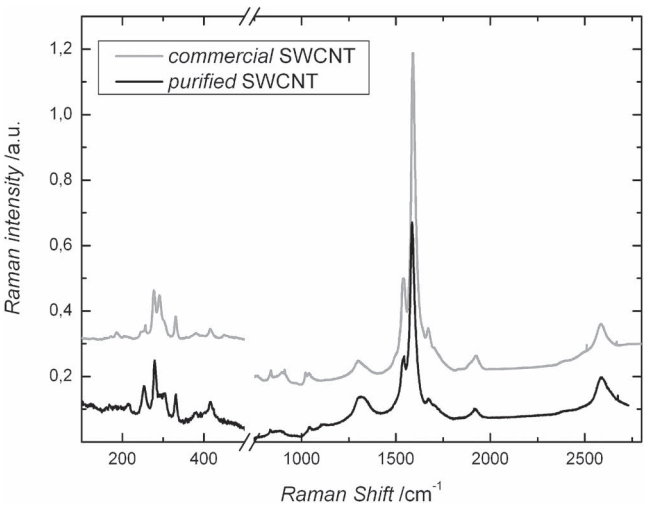

Figure 3. Raman spectra of the commercial (grey line) and purified (black line) samples. The spectra in the low-energy region are magnified to better resolve the RBM features.

reflection at $2\theta \approx 25°$ due to the carbon nanotubes. Both the XRPD and SEM analyses clearly show that the pristine sample was not homogeneous and presented not-negligible amounts of metallic impurities due to the synthesis method. Moreover, the nanotubes were organized in big bundles, which makes it difficult to disperse them in solvent. For these reasons, a purification step was required. Many methodologies have been reported in the literature,[10–12] but very often these procedures can break the single-walled nanotubes and also oxidize them, introducing functionalities. Therefore, in order to avoid these problems, we chose a soft purification process based on the use of a chelating agent to remove the catalysts.[13] The SEM image of the purified sample (Figure 1d) shows the nanotubes filaments emerging from aggregates, and Co and Mo crystallites are no longer visible. The XRPD pattern of this sample (Figure 2, trace b) presents only the typical peak of the carbon nanotubes at $2\theta \approx 25°$. In this way, the effectiveness of the purification has been proved.

For the characterization of the SWCNT-based samples, Raman spectroscopy has also been widely used. Besides the purity degree of the nanotubes, specific information concerning their diameter, electrical character, direction, and chirality can be derived from the parameters of the SWCNT Raman modes.[14–18] It is well known that these features are reflected in the main first- and second-order Raman modes, namely: i) the radial-breathing-mode (RBM) band (100–400 cm^{-1}). These signals are due to the Raman modes where all of the atoms of the tube vibrate radially in phase and, from the energies of the RBM, it is possible to estimate the tube diameter; ii) the D-band (1300–1400 cm^{-1}), also called the "disorder" band, which is related to the breathing motions of the sp^2 carbon atoms in rings, can be activated by the presence of defects on the nanotube surface, and generally reflects the presence of graphitic phase and amorphous carbon; iii) the G-band (1500–1600 cm^{-1}), also called the "tangential" mode, which consists of two subbands, G^+ and G^-, relating to the axial and circumferential in-plane vibrations, respectively, in semiconducting nanotubes; and iv) the 2D-band (2600–2800 cm^{-1}), which is the overtone of the D-band and is a fingerprint of the graphitic structure.

All of these features are clearly visible in the Raman spectra of the commercial and purified SWCNTs (**Figure 3**), even if with different relative intensities. The Raman spectra are consistent with the SW character of CNTs, as indicated by the strong G-band with the $G^{\pm}$ splitting, and the presence of the sharp RBM features. The effect of purification is clearly seen with the decrease or disappearance of the spurious Raman bands in the 700–900 cm^{-1} region, originating in the commercial sample from impurity phases.

The I_G/I_D ratio is a good marker of the disorder degree in SWCNTs. In our case, a decrease of the I_G/I_D ratio in the purified sample with respect to the commercial one (3.1 with respect to 6.8) was observed, thus indicating that the purification treatment had a not-negligible effect on the structure of the SWCNTs, causing an increase of the disorder degree. In any case, the I_G/I_D value of the purified sample is characteristic of high-quality SWCNTs with a low amount of amorphous carbon and/or other defects.[16,17]

In addition, the diameter (d_t (nm)) of the SWCNTs can be estimated from the frequency (ω_{RBM}, cm^{-1}) of the RBM by the equation $\omega_{RBM} = A/d_t + B$, where A and B are empirically found to be 223.5 nm cm^{-1} and 12.5 cm^{-1} for SWCNTs.[14] We obtained a d_t value of 0.84 nm from the most-intense RBM peak (ω_{RBM} = 280 cm^{-1}), thus consistent with that given by the supplier.

Similar analyses were performed on SWCNTs deposited on the glass substrate by the evaporation method. The Raman spectrum is reported in **Figure 4**a; a comparison between the spectrum of the purified powder and of the SA is shown in Figure 4b. For the SWCNTs on quartz glass, a non-symmetric shape and a broadening of the G-band at lower energies with respect to the purified sample were observed. This change is commonly attributed to a Breit–Wigner–Fano (BWF) resonance of metallic SWCNTs, induced by a coupling of the phonon excitation to a continuum of plasmon states.

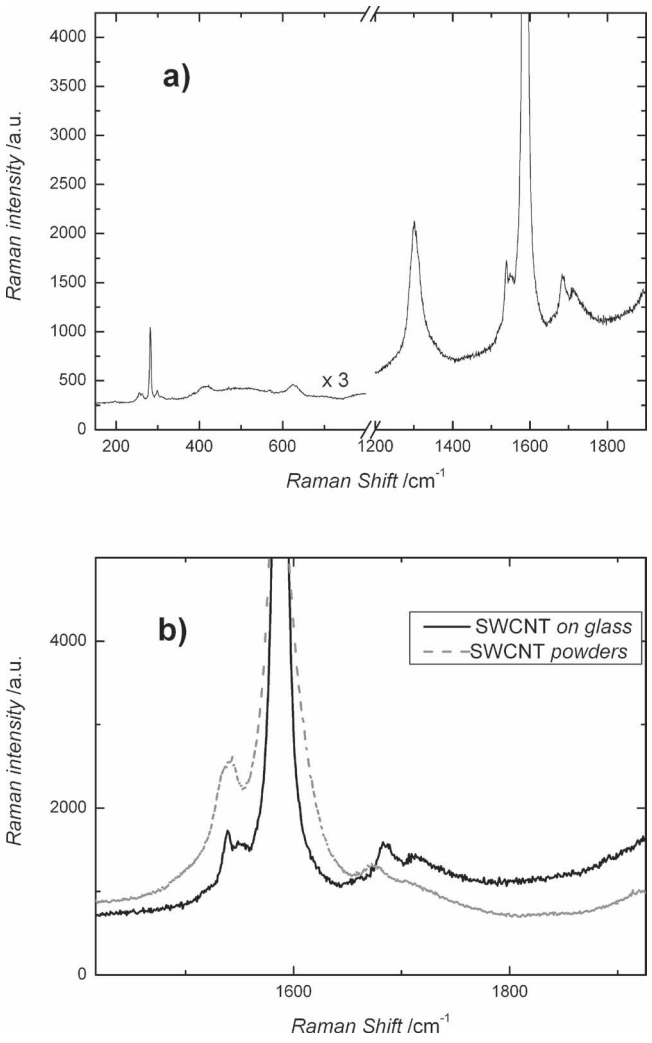

Figure 4. a) Raman spectrum of SWCNTs deposited on the hydrophilic quartz substrate. b) Details of the G band of the purified SWCNT powder and SWCNTs deposited on glass.

Indeed, the BWF feature was practically absent in the purified sample, according to the net semiconducting character of the starting materials. This character was retained by the SWCNTs deposited on glass, even though the appearance of a weak BWF shoulder was clearly appreciable (Figure 4b). This behavior indicates that an electron transfer from the vitreous matrix to the nanotubes accompanied the deposition process, increasing the metallic character of the nanotubes. It has been reported that metallic nanotubes can play a favorable role in SA functioning, because they can act as recombination centers, leading to a fast laser response.[19]

The tube-diameter value was also calculated for the deposited SWCNTs from the detailed analysis of the RBM structure (Figure 4a). From the energy of the three main RBM peaks and according to the formula reported above, we obtained diameter values of 0.92, 0.83, and 0.75 nm, with the intermediate value as the highly prevalent one.

Information regarding the directional properties of the deposited nanotubes can be obtained from polarized Raman

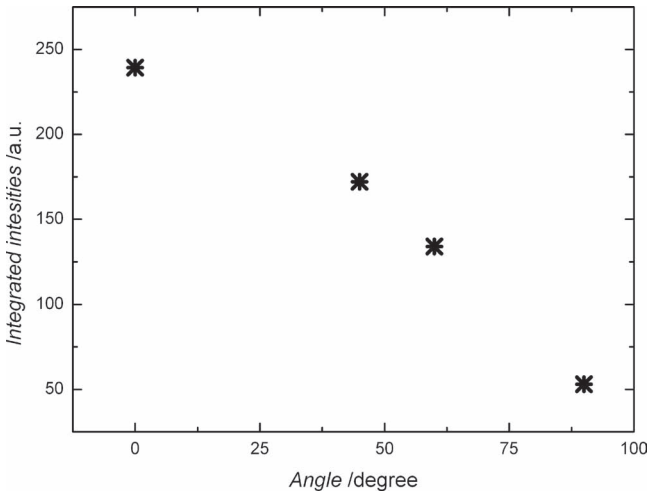

Figure 5. Integrated intensity of the whole spectrum in the range 1200–1800 cm^{-1} as a function of the rotation angle (see Experimental Section).

spectroscopy.[20–22] In fact, the Raman response of the aligned SWCNTs exhibited a marked dependence on the light-scattering geometry, with a strong decrease of all of the Raman features passing from the configuration where the light polarization was aligned to the tube axis with a transverse geometry. In our case, we obtained qualitative information, due to the fact that we measured the Raman response from a region containing several SWCNTs, and thus we could deduce a sort of depolarization ratio. Typical results are reported in **Figure 5**, where the integrated intensities for the whole spectrum in the range 1200–1800 cm^{-1} are reported as a function of the relative rotation angle of the same nanotube cluster with respect to VV geometry (see Experimental Section). A marked change with the light polarization is clearly evident, thus indicating the prevalence of aligned nanotubes.

The CNT film was tested as a SA in a Nd:glass femtosecond laser. Firstly, we measured the total losses (saturable + non-saturable) introduced by the SWCNT-SA employed in the mode-locking experiments. To this purpose, a Findlay–Clay analysis of the continuous-wave (cw) resonator depicted in **Figure 6** was carried out.[23] We investigated preliminarily the losses of the resonator operating without the SWCNT-SA; then, we

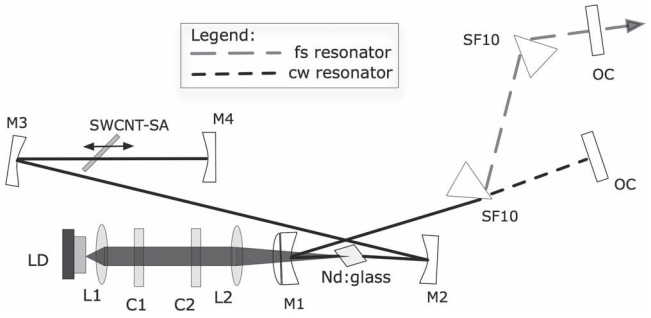

Figure 6. Experimental setup of the Nd:glass laser. OC: output coupler; SF10: dispersing isosceles prisms; M1–M4: spherical mirrors; C1 and C2: cylindrical lens telescope; L1 and L2: spherical lenses (refer to text for detailed list of the specifications for each component).

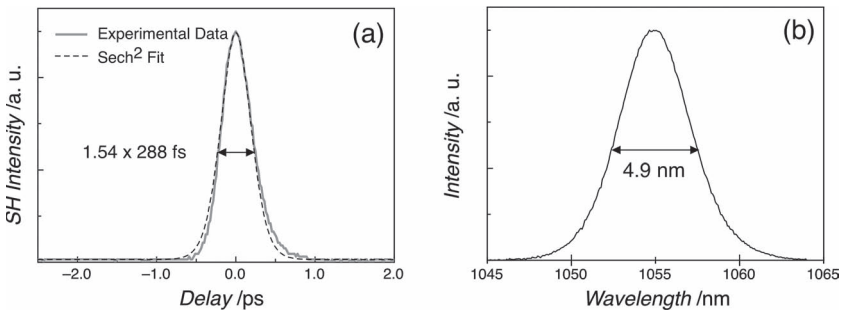

Figure 7. a) Mode-locked pulse-train autocorrelation trace. b) Corresponding optical spectrum.

inserted the sample and repeated the same measurements. In this way we were able to separate the contributions to the total cavity losses given by the resonator itself and the sample. The saturable + non-saturable losses introduced by the SWCNT-SA turned out to be about 1.7%, perfectly in the range of values also employed for SESAMs.[8,9]

Subsequently, we inserted SF10 dispersive prisms and switched to the cavity configuration for the femtosecond soliton mode-locking regime, as shown in Figure 6. We readily observed a stable mode-locking pulse train. Although the regime was not self-starting, if interrupted, mode-locking could be restored by gently shaking one of the mirror mounts or moving a prism. The pulse spectrum progressively broadened and the corresponding pulse duration shortened by moving the sample to the focus between the M3 and M4 curved mirrors. Employing an output coupler with transmittivity $T = 0.4\%$, we obtained pulses as short as 288 fs with full width at half-maximum (FWHM) spectra 4.9 nm wide centered around 1055 nm (**Figure 7**) and having an average output power of 18 mW. The pulse was nearly Fourier limited with a time-bandwidth product of 0.38 (0.32 for the ideal *sech*^{2} intensity pulse-shape), as usually turns out in the soliton regime.

It is worth noting that, to the best of our knowledge, these are the shortest pulses that have been reported in the literature for an ultrafast laser mode-locked with a SWCNT-SA realized using the evaporation technique. Earlier results with femtosecond Nd:phosphate lasers and polymer-embedded carbon nanotubes have been obtained using saturable-absorber mirrors (≈200 fs)[24] whereas the shortest pulses of 99 fs were achieved recently using Nd:silicate.[25] In particular, for that result, the optimization of the modulation depth of the absorber was critical. It is believed that further work in this direction will allow also the evaporation method to match such performance.

In **Figure 8**, we report the radio frequency of the cw-mode-locked pulse train, indicating no sidebands and therefore no amplitude-modulation instabilities.

Subsequently, we tested several different output couplers in order to investigate the maximum output power and corresponding pulse duration that we could obtain. The results are summarized in **Table 1**. As expected, the pulse broadened on reducing the intracavity pulse energy, with a larger output coupling allowing a higher output power. A maximum average output power of 60 mW was obtained with 500 fs-long pulses employing a $T = 2.4\%$ output coupler. For comparison, the laser emitted a maximum power of 170 mW in cw operation. The efficiency reduction observed in the mode-locking regime was most likely due to non-saturable losses introduced by the SWCNT-SA.

The performed tests allowed us to prove that the previously described characteristics make our sample suitable for femtosecond mode-locking in solid-state lasers with near 1 μm wavelength. In order to assess the full potential of the power scalability and the femtosecond operation with these new saturable absorbers, a further experiment is planned using an Yb laser, definitely more suitable than Nd:glass to this aim. A pump and probe setup[26] could help for direct measurement of the saturation fluence, the modulation depth, and the response time of the SWCNT-SA sample, and a preliminary experiment with a 150 fs laser at 1060 nm has confirmed an ultrafast relaxation time of the SWCNT-SA of about 180 fs (**Figure 9**). Unfortunately, the modulation depth was too small to determine its value with the pump-and-probe setup directly; therefore, the saturation fluence could not be measured. However, since stable femtosecond generation occurred within a range of parameters, such as pulse energy and spot size, comparable with earlier experiments with Nd:glass, we expect that the saturation fluence would be similar to that of other SWCNT-SAs that have been demonstrated previously (i.e., ≈10–100 μJ cm^{-2}).

Only the total insertion loss could be inferred by the Findlay–Clay analysis; certainly, it is more difficult to measure it directly, for example with the Z-scan technique,[27] without lock-in amplifiers. In principle, a successful demonstration of an ultrafast Nd:glass laser could be expected from the first reports on SWCNT-SAs fabricated using the evaporation technique,[6] where the absorbers were fully characterized. However, it is not a trivial task to realize the sufficiently

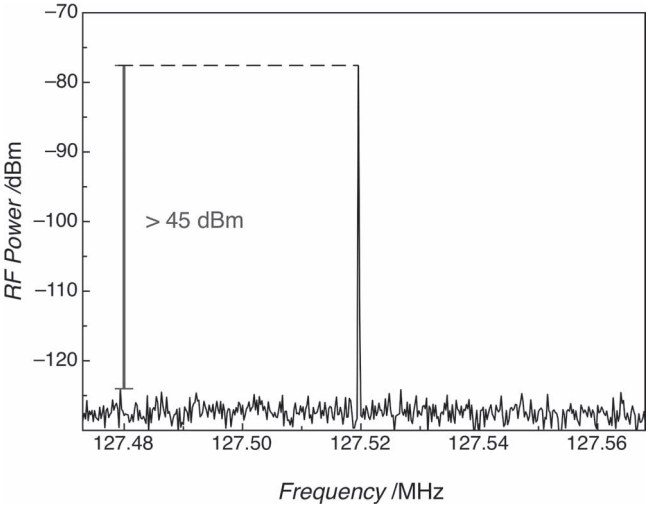

Figure 8. The radio frequency spectrum of the cw mode-locked pulse train.

Table 1. Maximum output power, pulse duration, and FWHM of the optical spectrum for different output couplers.

OC transmission [%]	Maximum power [mW]	Pulse duration [fs]	Spectrum FWHM [nm]
0.4	18	288	4.9
0.8	30	380	3.7
1.6	43	420	3.2
2.4	60	500	2.0

small insertion loss required for the mode-locking of a low-gain medium such as Nd:glass, and at the same time provide sufficient non-linear modulation to sustain the pulse formation. Therefore, a new, interesting result emerging from our research is that the evaporation method is also suitable for the fabrication of relatively low-loss SWCNT-SAs. This low loss can be related to the statistical alignment distribution of the deposited nanotubes, as demonstrated by light-polarization Raman spectroscopy.

3. Conclusions

Femtosecond operation of a solid-state diode-pumped Nd:glass laser has been demonstrated using SWCNT-SAs fabricated by the evaporation method, showing that this fabrication technique is suitable for mode-locking low-gain solid-state ultrafast lasers such as ytterbium lasers, which tolerate low intracavity losses. The simplicity and the effectiveness of these SWCNT-SAs is very promising for further development of valid alternatives to SESAMs. The purification process, the good quality of the aqueous dispersion, and the SWCNTs alignment on the glass substrate have been demonstrated to be of great importance for the preparation of SAs applied in solid-state ultrafast lasers.

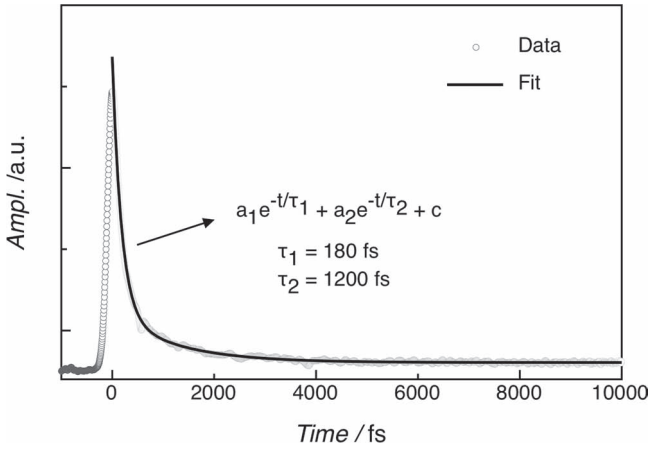

Figure 9. Pump and probe measurements of the SWCNT-SA relaxation time: the curve has been fitted with a double-exponential with fast (180 fs) and slower (1.2 ps) responses.

4. Experimental Section

SWCNTs were purchased from South West NanoTechnologies Inc., SG65 type CoMoCat. The average diameter declared by the supplier was 0.8 ± 0.1 nm and more than 90% of tubes were semiconducting. The purification of the SWCNTs was performed by using the non-destructive methodology proposed by Wang et al.[13] After thermal treatment in air at 200 °C, the nanotubes were dispersed in deionized water, ultrasonicated, and then a 0.5 M solution of *trans*-1,2-diaminocyclohexane-*N*,*N*,*N*′,*N*′-tetra-acetic acid (CYDTA) (Fluka Idranal IV) was added, and the mixture was refluxed at 110 °C for 18 h. The obtained suspension was then filtered and washed several times with hot water.

The purified nanotubes (0.6 mg) were then used for the preparation of an aqueous dispersion (10 ml) using sodium dodecyl sulfate (SDS) as a surfactant (≈10^{-3} M). This dispersion was ultrasonicated for 6 h and then centrifuged at 13 000 g, overall for 1.5 h, with intermediate sampling of the supernatant. Quartz glass, made hydrophilic by using NaOH (0.5 M), was inserted vertically in the final dispersion, and the solvent was evaporated slowly (for about three weeks) at ambient temperature.[28]

Room-temperature (r.t.) XRPD measurements were performed in air using a Bruker D5005 diffractometer with Cu K_α radiation, a Ni filter, and a position-sensitive detector (PSD).

SEM measurements and EDS analysis were performed using a Zeiss EVO-MA10-HR microscope.

Micro-Raman spectroscopy measurements were carried out using a Labram Dilor Raman H10 spectrometer equipped with an Olympus microscope HS BX40 objective and with a cooled CCD camera as the photodetector. 632.8 nm (1.96 eV) light from a He-Ne laser was used as the excitation radiation. A 100× objective (NA = 0.99) was normally used, with a spatial resolution slightly smaller than 1 μm. The power density incident on the sample was ≈1 μW μm^{-2} so that heating effects could be neglected. All of the measurements were made at r.t. in backscattering geometry. The typical integration time was 60 s. The parameters of the Raman modes were obtained by applying best-fit procedures to interpolate the measured experimental peaks, using Lorentzian curves as the fitting function. Measurements with polarized light were made using the VV configuration, with the polarization direction parallel to the microscope plate and rotating the deposited glass around the optical axis. For these measurements, three clusters of the deposited film were analyzed.

The experimental setup for the laser tests is depicted in Figure 6. The pump diode was a 50 μm × 1 μm broad-area emitter (Frankfurt Laser Company, GmbH), emitting a maximum output power of 1 W at 805 nm. The laser diode was collimated by an 8 mm focal aspheric lens L1, expanded by a factor of 15× in the slow-axis direction with a cylindrical-lens telescope (C1, C2), and was eventually focused in the 4 mm-long Brewster cut N31 phosphate glass sample by the 75 mm focal achromat L2.

A CCD camera was employed to characterize the pump-beam profile in the focal region of the optical system during the alignment of the pump telescope. We measured a pump-beam waist radius $w_x \times w_y$ of 16 μm × 11 μm and $M^2_x = 6.5$, $M^2_y = 2$. The active medium was contacted to a metallic plate without any active cooling. In order to compensate for cavity-mode astigmatism, the M1 and M2 folding angles were set to about 7°, whereas the separation between M1 and M2 was chosen to be ≈105 mm in order to operate the resonator near the center of its stability range. The lengths of the cavity arms M2–M3 and M3–M4 were about 320 and 150 mm, respectively. All of the spherical mirrors M1-M4 had a radius of curvature of 100 mm. The distance between the two SF10 dispersing isosceles prisms was set to 260 mm in order to operate the resonator in the net-negative intracavity group-velocity-dispersion (GVD) regime, required for stable soliton mode-locking. The SWCNT-SA plate was oriented at the Brewster angle in order to minimize insertion losses and was mounted on a translation stage in order to scan the focal region between the spherical mirrors M3 and M4, hence varying the beam size over the sample. The transverse position of the beam on the saturable absorber could be also scanned using a second micrometric translation stage. The waist-mode radius in the Nd:glass and in the focus between

mirrors M3 and M4 was ≈25–30 μm, as computed by the usual ABCD beam-propagation methods.

Acknowledgements

This research received funding from Cariplo Foundation under grant agreement No. 2009–2309.

Received: January 17, 2012
Revised: April 27, 2012
Published online: June 15, 2012

[1] U. Keller, *Nature* **2003**, *424*, 831.
[2] S. Y. Set, H. Yaguchi, Y. Tanaka, M. Jablonski, *IEEE J. Quantum Electron.* **2004**, *10*, 137.
[3] W. B. Cho, J. H. Yim, S. Y. Choi, S. Lee, A. Schmidt, G. Steinmeyer, U. Griebner, V. Petrov, D.-I. Yeom, K. Kim, F. Rotermund, *Adv. Funct. Mater.* **2010**, *20*, 1937.
[4] T. Hasan, Z. Sun, F. Wang, F. Bonaccorso, P. H. Tan, A. G. Rozhin, A. C. Ferrari, *Adv. Mater.* **2009**, *21*, 3874.
[5] S. Kivistö, T. Hakulinen, A. Kaskela, B. Aitchison, D. P. Brown, A. G. Nasibulin, E. I. Kauppinen, A. Härkönen, O. G. Okhotnikov, *Opt. Express* **2009**, *17*, 2358.
[6] Y. G. Wang, X. Y. Ma, *Laser Phys.* **2011**, *21*, 148.
[7] H. R. Chen, Y. G. Wang, C. Y. Tsai, K. H. Lin, T. Y. Chang, J. Tang, W. F. Hsieh, *Opt. Lett.* **2011**, *36*, 1284.
[8] U. Keller, T. H. Chiu, J. F. Ferguson, *Opt. Lett.* **1993**,*18*, 1077.
[9] A. Agnesi, A. Greborio, F. Pirzio, E. Ugolotti, G. Reali, S. Y. Choi, F. Rotermund, U. Griebner, V. Petrov, *IEEE J. Quantum Electron.* **2012**, *18*, 74.
[10] P.-X. Hou, C. Liu, H.-M. Cheng, *Carbon* **2008**, *46*, 2003.
[11] J. Ma, J. N. Wang, *Chem. Mater.* **2008**, *20*, 2895.
[12] S. Fogden, R. Verdejo, B. Cottam, M. Shaffer, *Chem. Phys. Lett.* **2008**, *460*, 162.
[13] Y. Wang, L. Huang, Y. Liu, D. Wei, H. Zhang, H. Kajiura, Y. Li, *Nano Res.* **2009**, *2*, 865.
[14] M. S. Dresselhaus, G. Dresselhaus, P. Avouris, *Carbon Nanotubes: Synthesis, Structure, Properties, and Applications*, Springer-Verlag, Berlin **2001.**
[15] M. S. Dresselhaus, P. C. Eklund, *Adv. Phys.* **2000**, *49*, 705.
[16] R. Saito, T. Takeya, T. Kimura, G. Dresselhaus, M. S. Dresselhaus, *Phys. Rev. B: Condens. Matter* **1998**, *57*, 4145.
[17] M. S. Dresselhaus, G. Dresselhaus, R. Saito, A. Jorio, *Phys. Rep.* **2005**, *409*, 47.
[18] M. S. Dresselhaus, A. Jorio, M. Hofmann, G. Dresselhaus, R. Saito, *Nano Lett.* **2010**, *10*, 751.
[19] J.-S. Lauret, C. Voisin, G. Cassabois, C. Delalande, P. Roussignol, O. Jos, L. Capes, *Phys. Rev. Lett.* **2003**, *90*, 057404.
[20] J. Hwang, H. H. Gommans, A. Ugawa, H. Tashiro, R. Haggenmueller, K. I. Winey, J. E. Fischer, D. B. Tanner, A. G. Rinzler, *Phys. Rev. B: Condens. Matter* **2000**, *62*, R13 310.
[21] L. Gomez-De Arco, B. Lei, S. Cronin, C. Zhou, *Appl. Phys. Lett.* **2008**, *93*, 123112.
[22] H. H. Gommans, J. W. Alldredge, H. Tashiro, J. Park, J. Magnuson, A. G. Rinzlerd, *J. Appl. Phys.* **2000**, *88*, 2509.
[23] D. Findlay, R. A. Clay, *Phys. Lett.* **1966**, *20*, 277.
[24] T. R. Schibli, K. Minoshima, H. Kataura, E. Itoga, N. Minami, S. Kazaoui, K. Miyashita, M. Tokumoto, Y. Sakakibara, *Opt. Express* **2005**, *13*, 8025.
[25] A. Agnesi, A. Greborio, F. Pirzio, G. Reali, S. Y. Choi, F. Rotermund, U. Griebner, V. Petrov, *Appl. Phys. Express* **2010**, *3*, 112702.
[26] J. H. Yim, W. B. Cho, S. Lee, Y. H. Ahn, K. Kim, H. Lim, G. Steinmeyer, V. Petrov, U. Griebner, F. Rotermund, *Appl. Phys. Lett.* **2008**, *93*, 161106.
[27] M. Sheik-Bahae, A. A. Said, E. W. Van Stryland, *Opt. Lett.* **1989**, *14*, 955.
[28] Y. G. Wang, X. Y. Ma, *Laser Phys.* **2011**, *21*, 148.